Adaptive Speed Control for Linear Induction Motors Considering End Effect

Kuang-Yow Lian, Cheng-Yao Hung
Department of Electrical Engineering
Chung-Yuan Christian University
Chung-Li 32023, Taiwan
TEL: 886-3-2654815
FAX: 886-3-2654899
Email: lian@dec.ee.cycu.edu.tw

Li-Chen Fu
Department of Electrical Engineering
National Taiwan University
Taipei, Taiwan
Email: lichen@ccms.ntu.edu.tw

Keywords: Linear induction motors, end effects, adaptive speed control.

Abstract

In this paper, the speed control problem of linear induction motors is considered based on a *semi-current-fed* model. Once deriving the mathematical model considering end effects, adaptive control design is developed by using so-called virtual desired variable synthesis. Based on the synthesis method, the control law is naturally deduced while thrust load and mechanical parameters are unknown. Finally, practical experiments for linear induction motors are carried out to verify the theoretical derivations.

Nomenclature

$V_{sa}(V_{sb})$	a-axis(b-axis) primary voltage
$i_{sa}(i_{sb})$	a-axis(b-axis) primary current
$\lambda_{ra}(\lambda_{rb})$	a-axis(b-axis) secondary flux
$R_s(R_r)$	primary(secondary) resistance
$L_s(L_r)$	primary(secondary) inductance
L_m	magnetizing inductance
M	primary mass
D	viscous friction coefficient
n_p	number of pole pairs
τ	pole pitch
F	electromagnetic thrust

1. Introduction

Linear induction motors (LIM) are important devices in industrial applications due to their high reliability, minimal mechanical loss, easy maintenance, high-initial thrust, and less noise. The structure of an LIM is like an induction motor (IM) cut open and rolled flat. Thus, the driver of an LIM is similar to the traditional IM. However, for LIMs we need to consider the end effect, which occurs at the entry and exit areas due to sudden change of fluxes [1]. The end effect is an important feature while designing the controller, but many works in previous literature lacks consideration. In this paper, the end effect is modeled and considered in controller design. According to the model of a three-phase LIM, a fifth-order model is given with respect to a fixed reference frame attached to the stator. Combining the end effects [5], we obtain the complete mathematical model of an LIM. Based on this model, we develop an output feedback algorithm to achieve speed and flux regulation in spite of unknown time-varying thrust load.

In this paper, we consider the speed tracking control problem for LIMs based on a newly proposed *semi-current-fed* model [3]. This model has relaxed assumptions compared to the typical current-fed model [4]. Here we either assume the current-loop maintains the primary voltage upper bounded and/or that the L_1 norm of the current tracking error is bounded. This approach is in contrast to the previous works on current-fed models where an ideal current-loop control is assumed. For the problem formulation of speed tracking, only the primary speed, primary voltage and current are measurable whereas thrust load is unknown. In adaptive controller synthesis, a set of virtual desired variables (VDV) is utilized and denoted to be desired secondary fluxes. The VDVs are determined in a straightforward manner once considering the principal objectives of vector control the intention of achieving a well performing current regulator and exact field orientation. To avoid using secondary flux feedback, an auxiliary signal is imposed to relate the secondary flux error to the measurable signals. From stability analysis, the proposed adaptive controller is able to achieve asymptotic speed tracking. In addition, the flux tracking is achieved if condition of persistent excitation is satisfied [2].

2. Dynamical model of linear induction motors with end effect

The structure of an LIM is similar to the IM. The primary is the same as a flat stator of IM. The secondary consists of a sheet conductor with an iron return path for the magnetic flux. Therefore $\theta = \frac{\pi}{\tau} d$, $\omega = \frac{\pi}{\tau} v$.

The model of a three-phase LIM without considering end effect is represented by the fifth-order model:

$$\beta \dot{\mathbf{i}} + \Phi_1 \mathbf{i} + \Theta \boldsymbol{\lambda} = \frac{L_r}{L_m} \mathbf{V}_s \quad (1)$$

$$\dot{\boldsymbol{\lambda}} - \Theta \boldsymbol{\lambda} - \frac{L_m R_r}{L_r} \mathbf{i} = 0 \quad (2)$$

$$M\dot{v} + Bv = F - F_l \quad (3)$$

$$F = \frac{n_p L_m}{L_r}\mathbf{i}^{\mathrm{T}}\mathbf{J}_2\boldsymbol{\lambda} \quad (4)$$

where $\Phi_1 = \frac{L_r R_s}{L_m} + \frac{L_m R_r}{L_r}$, $\Theta = \frac{\pi}{\tau}v\mathbf{J}_2 - \frac{R_r}{L_r}\mathbf{I}_2$, $\beta = \frac{\sigma L_r}{L_m}$, $\sigma = L_s - L_m^2/L_r$, $\mathbf{i} = [i_{sa}\ i_{sb}]^{\mathrm{T}}$, $\boldsymbol{\lambda} = [\lambda_{ra}\ \lambda_{rb}]^{\mathrm{T}}$, $\mathbf{V}_s = [V_{sa}\ V_{sb}]^{\mathrm{T}}$, $\mathbf{I}_2 = diag\{1, 1\}$, $\mathbf{J}_2 = \begin{bmatrix} 0 & -1 \\ 1 & 0 \end{bmatrix}$. The scalar function F represents the electromechanical coupling thrust, which is expressed as $F = \frac{n_p L_m}{L_r}(\lambda_{ra} i_{sb} - \lambda_{rb} i_{sa})$, where n_p denotes one and a half the pole pair number. For an LIM, when the primary moves, the magnetism of the secondary at the entry area will tend to resist a sudden increase in flux penetration and only allow a gradual build up of the flux density in the air gap. An equivalent circuit model is developed for LIM by adding the end effect. When primary moves, a new field penetrates into the reaction rail in the entry area, whereas the existing field disappears at the exist area of the primary. The eddy current grows very rapidly to mirror the primary current. On the other hand, the eddy current at the exit generates a kind of weak field, dragging the moving motion of the primary. When we do not consider the end effect, the entry flux can be expressed as:

$$\begin{aligned} \boldsymbol{\lambda}_{entry} &= [\ \lambda_u \cos(120^0) \quad \lambda_v \cos(240^0) \quad \lambda_w\ ]^{\mathrm{T}} \\ &= [\ -\tfrac{1}{2}\lambda_u \quad \tfrac{1}{2}\lambda_v \quad \lambda_w\ ]^{\mathrm{T}}. \end{aligned}$$

Because $(\mathbf{i}^{\varepsilon}_{entry})_{\max} \propto \boldsymbol{\lambda}_{entry}$, we obtain $(\mathbf{i}^{\varepsilon}_{entry})_{\max} = [\ -\frac{1}{2}i_{su} \quad -\frac{1}{2}i_{sv} \quad i_{sw}\ ]^{\mathrm{T}}$, where $(\mathbf{i}^{\varepsilon}_{entry})_{\max}$ is transferred into the orthogonal two-dimension coordinate system and expressed as $(\mathbf{i}^{\varepsilon}_{entry})_{\max} = \left[\ \chi i_{sa} \quad \chi i_{sb}\ \right]^{\mathrm{T}}$. Therefore, the entry eddy current decays with respect to time

$$(\mathbf{i}^{\varepsilon}_{entry})_{dec} = \left[\ \chi i_{sa} e^{-\frac{t}{T_r}} \quad \chi i_{sb} e^{-\frac{t}{T_r}}\ \right]^{\mathrm{T}}$$

where $T_r = \frac{L_r}{R_r}$. The averaged current leads to

$$\mathbf{i}^{\varepsilon}_{entry} = \left[\ \frac{1}{T_v}\chi i_{sa}\int_0^{T_v} e^{-\frac{t}{T_r}}dt \quad \chi i_{sb}\int_0^{T_v} e^{-\frac{t}{T_r}}dt\ \right]^{\mathrm{T}}$$

where $T_v = \frac{D_l}{v}$ and D_l is the primary length. Define $\Upsilon = \frac{v \times T_v}{v \times T_r} = \frac{D_l R_r}{L_r v}$, where Υ a is dimensionless constant. Therefore,

$$\mathbf{i}^{\varepsilon}_{entry} = [\ \chi i_{sa} f(\Upsilon) \quad \chi i_{sb} f(\Upsilon)\ ]^{\mathrm{T}} \quad (5)$$

where $f(\Upsilon) = \frac{1-e^{-\Upsilon}}{\Upsilon}$, $x = \frac{t}{T_r}$. The effective magnetizing current is reduced to

$$\mathbf{i}_s^{eq} = \left[\ [1 + \chi f(\Upsilon)] i_{sa} \quad [1 + \chi f(\Upsilon)] i_{sb}\ \right]^{\mathrm{T}}.$$

Consequently, the flux due to the eddy current can be accounted by modifying

$$\begin{aligned} \boldsymbol{\lambda}_s &= L_s[1 + \chi f(\Upsilon)]\mathbf{i}_s + L_m\mathbf{i}_r \\ \boldsymbol{\lambda}_r &= L_r\mathbf{i}_r + L_m[1 + \chi f(\Upsilon)]\mathbf{i}_s. \end{aligned}$$

On the other hand, we see the end effect as the influence of the magnetizing inductance. Note that the root mean square (RMS) value of the eddy current over the primary length is given by $(\mathbf{i}^{\varepsilon}_{entry})_{rms} = (\mathbf{i}^{\varepsilon}_{entry})_{\max}\left(\frac{1-e^{-2\Upsilon}}{2\Upsilon}\right)^{\frac{1}{2}}$. The loss caused by the entry eddy current is expressed as:

$$P_{entry} = \chi^2(\tfrac{1-e^{-2\Upsilon}}{2\Upsilon})i_{sa}^2 R_r + \chi^2(\tfrac{1-e^{-2\Upsilon}}{2\Upsilon})i_{sb}^2 R_r \quad (6)$$

according to

$$(\mathbf{i}^{\varepsilon}_{entry})_{total} = [\ \chi i_{sa}(1 - e^{-\Upsilon}) \quad \chi i_{sb}(1 - e^{-\Upsilon})\ ]^{\mathrm{T}}.$$

The loss caused by the exit eddy current is expressed as:

$$P_{exit} = \tfrac{R_r}{2\Upsilon}(1 - e^{-\Upsilon})^2\chi^2\left[i_{sa}^2 + i_{sb}^2\right]. \quad (7)$$

Summing (6) and (7), the total loss due to eddy current is expressed $P_{entry} + P_{exit} = i_{sa}^2\left[R_r\chi^2 f(\Upsilon)\right] + i_{sb}^2\left[R_r\chi^2 f(\Upsilon)\right]$. The model (1)$\sim$(4) above can be expressed in a vector form:

$$\begin{aligned} \beta p(\alpha_2\mathbf{i}) + \Phi\mathbf{i} + \Theta\boldsymbol{\lambda} &= \tfrac{L_r}{L_m}\mathbf{V}_s & (8)\\ p(\boldsymbol{\lambda}) - \Theta\boldsymbol{\lambda} - \tfrac{L_m R_r}{L_r}\alpha_2\mathbf{i} &= 0 & (9)\\ Mp(v) + Dv &= F - F_l & (10)\\ F &= \frac{\pi n_p L_m}{\tau L_r}\alpha_2\mathbf{i}^{\mathrm{T}}\mathbf{J}_2\boldsymbol{\lambda}. & (11) \end{aligned}$$

where $\Phi = \frac{L_r R_s}{L_m} + \frac{L_m R_r}{L_r}\alpha_2 + \frac{L_r}{L_m}\alpha_1$, $\alpha_1 = R_r\chi^2 f(\Upsilon)$, $\alpha_2 = 1 + \chi f(\Upsilon)$.

3. Problem formulation

In practical current-fed model, high-gain PI current loops are imposed to regulate the primary currents. The concise block diagram of a practical current-fed model system is shown in Fig. 1. The block diagram illustrates that the primary currents (i_{sa}, i_{sb}) are forced to track the reference signals (i_{sa}^*, i_{sb}^*) by virtue of the PI control input defined as follows:

$$\begin{aligned} V_{sa} &= -K_{ap}\widetilde{i}_{sa} - K_{ai}\int_0^t \widetilde{i}_{sa}dt & (12)\\ V_{sb} &= -K_{bp}\widetilde{i}_{sb} - K_{bi}\int_0^t \widetilde{i}_{sb}dt & (13) \end{aligned}$$

where $\widetilde{i}_{sa} = i_{sa} - i_{sa}^*$, $\widetilde{i}_{sb} = i_{sb} - i_{sb}^*$, and the positive gains K_{ap}, K_{ai}, K_{bp}, K_{bi} are properly chosen such that the current loop has satisfactory performance. Therefore, the dynamics of the primary currents (8) are neglected and the reference signals of the primary are regarded as the control inputs. In other words, we replace $\mathbf{i}$ with $\mathbf{i}^*$. Finally, the reduced-order model of the LIM is expressed by (9) and (10). However, due to current loop uncertainties and saturation induced by high-gain control, the assumption of an ideal current loop control in practical situations is not easily satisfied. To cope with this problem, a semi-current-fed concept is stated in the following assumptions:

A.1: By proper choice of PI gains in (12) and (13), the current loop performs well such that $\mathbf{V}_s$ is bounded, i.e., $\mathbf{V}_s \in L_\infty$.

Since (12) and (13) is taken here as a stable filter driven by $\mathbf{V}_s$, we have $\widetilde{i}_{sa}, \widetilde{i}_{sb} \in L_\infty$ according to A.1. A stronger assumption is made as follows:

A.1': In addition to A.1, the current tracking errors are assumed to be a finite integrable function, i.e., $\widetilde{i}_{sa}, \widetilde{i}_{sb} \in L_\infty \cap L_1$.

Under the sense of A.1 or A.1', we call this current controlled LIM as a *semi-current-fed* LIM. This terminology arises from the fact that A.1 and A.1' relaxes the assumption $i_{sa} = i^*_{sa}$, $i_{sb} = i^*_{sb}$, which has been needed in typical current-fed model control. Therefore the speed control design based on a semi-current-fed concept is a step closer to practical situations. Before the controller synthesis, some other assumptions are given:

A.2 The voltages and currents of primary, along with the speed of primary are considered to be measurable.

A.3 Mass of primary M and viscous friction coefficient D are unknown constants.

A.4 The parameters L_m, L_r, R_s, R_r are known constants.

A.5 The load thrust F_l can be parameterized as

$$F_l = \begin{bmatrix} 1 & v & v^2 \end{bmatrix} \begin{bmatrix} \theta_1 & \theta_2 & \theta_3 \end{bmatrix}^{\mathrm{T}} \equiv \mathbf{Y}_v \boldsymbol{\theta}_v$$

where θ_1 is the constant load in normal operation conditions and θ_2, θ_3 are coefficients of the various loads.

A.6 The desired speed v_d is a smooth and bounded function.

4. Design method of virtual desired variables

4.1 Mechanical loop control

First, consider the mechanical dynamics (10). The speed tracking error $\tilde{v} \equiv v - v_d$. Therefore, (10) is rewritten in terms of $\tilde{v}$ as follows:

$$M\dot{\tilde{v}} + (D + k_v)\,\tilde{v} = F - F_d + (F_d - \mathbf{Y}\boldsymbol{\theta} + k_v\tilde{v}) \tag{14}$$

where F_d denotes the desired thrust which produces the desired speed; k_v is a adjustable damping ratio; $\mathbf{Y} = [\mathbf{Y}_v \ \dot{v}_d \ v_d]$ is a regression matrix; and $\boldsymbol{\theta} \equiv [\boldsymbol{\theta}_v^{\mathrm{T}} \ M \ D]^{\mathrm{T}}$ is a parameter vector. The damping term $k_v\tilde{v}$ plays a dominant role on the transient response for speed tracking. For speed tracking control, the desired thrust is naturally defined to be

$$F_d = \mathbf{Y}\widehat{\boldsymbol{\theta}} - k_v\tilde{v} \tag{15}$$

where $\widehat{\boldsymbol{\theta}}$ is the estimated vector of $\boldsymbol{\theta}$. Therefore the following error dynamics are obtained:

$$M\dot{\tilde{v}} + (D + k_v)\,\tilde{v} = F - F_d - \mathbf{Y}\widetilde{\boldsymbol{\theta}} \tag{16}$$

with the estimation error $\widetilde{\boldsymbol{\theta}} \equiv \boldsymbol{\theta} - \widehat{\boldsymbol{\theta}}$. The update laws for $\widehat{\boldsymbol{\theta}}$ will be properly chosen such that responding effect for the term containing $\widetilde{\boldsymbol{\theta}}$ is driven to zero. Therefore the primary speed will converge to the desired value at a desired rate based on a suitably chosen k_v if F approaches F_d. To this end, the speed tracking control problem has been reformulated into the thrust tracking problem. In other words, the remainder of the control design is to generate a thrust F to track the desired thrust F_d while all internal signals are maintained bounded. Consider the cascaded subsystems (8) and (9). The vector control problem is to design a desired current $\mathbf{i}^*$ and a desired flux $\boldsymbol{\lambda}_d$ independently such that the electrical subsystem can generate the desired thrust F_d. Here $\boldsymbol{\lambda}_d$ is a VDV for $\boldsymbol{\lambda}$. From the above statement and according to thrust equation (4), synthesize the following

$$F_d = \tfrac{\pi n_p L_m}{\tau L_r}\alpha_2 \mathbf{i}^{*\mathrm{T}}\mathbf{J}_2\boldsymbol{\lambda}_d \tag{17}$$

Once $\mathbf{i}$ and $\boldsymbol{\lambda}$ converge to $\mathbf{i}^*$ and $\boldsymbol{\lambda}_d$, F converges to F_d. Based on the semi-current-fed concept, the convergence of $\mathbf{i}$ to $\mathbf{i}^*$ depends on whether the current loop controller satisfies the assumptions A.1 or A.1'. Consequently, the objective of thrust tracking is reformulated into designing $\mathbf{i}^*$ and $\boldsymbol{\lambda}_d$ such that $\boldsymbol{\lambda} \to \boldsymbol{\lambda}_d$ while satisfying (17). In light of vector control analysis, we impose some conditions on the VDVs $\mathbf{i}^*$ and $\boldsymbol{\lambda}_d$. First, the optimal thrust will be obtained by setting the magnitude of magnetic flux to a constant value. To achieve this property, we let $\|\boldsymbol{\lambda}_d\| = c$, where c is a given constant. This further implies that the virtual desired flux in the primary frame is $\boldsymbol{\lambda}_d = (c\cos(\rho(t)) \ \ c\sin(\rho(t)))$, where $\rho(t)$ denotes the angle between the stator frame and excitation frame which is to be determined later. In light of the above, $\boldsymbol{\lambda}_d$ and $\mathbf{i}^*$ are constrained by the following conditions: **C.1** $\boldsymbol{\lambda}_d$ is kept constant by letting $\|\boldsymbol{\lambda}_d\| = c$; **C.2** $\boldsymbol{\lambda}_d$ and $\mathbf{i}^*$ satisfy (17). As a result, the control objective is to design $\mathbf{i}^*$ such that $\boldsymbol{\lambda} \to \boldsymbol{\lambda}_d$, where $\boldsymbol{\lambda}_d$ is constrained by C.1 and C.2.

4.2 Realization of VDV-synthesis

Since the secondary flux is not measurable, we omit the use of flux sensors and reconstruct the flux signals without using an observer. From (8) and (9), we have:

$$\beta p(\alpha_2\mathbf{i}) + p(\boldsymbol{\lambda}) = p(\boldsymbol{\eta}) \tag{18}$$

where $p(\boldsymbol{\eta}) = -(\frac{R_s L_r}{L_m} + \frac{L_r}{L_m}\alpha_1)\mathbf{i} + \frac{L_r}{L_m}\mathbf{V}_s$ is a first order filter. Integrating (18), the flux signals

$$\boldsymbol{\lambda} = \boldsymbol{\eta} - \beta\alpha_2\mathbf{i} + \mathbf{A} \tag{19}$$

where $\mathbf{A}$ is an unknown integration constant vector dependent on initial conditions. From (19), the reconstructed flux signals are expressed as $\widehat{\boldsymbol{\lambda}} = \boldsymbol{\eta} - \beta\alpha_2\mathbf{i} + \widehat{\mathbf{A}}$, where $\widehat{\mathbf{A}}$ is an estimated signal of $\mathbf{A}$ and is to be determined by the adaptive mechanism. The overall VDV-synthesis algorithm is given in the following:

Step 1 First, change the original flux tracking into the tracking of reconstructed flux $\widehat{\boldsymbol{\lambda}}$ to $\boldsymbol{\lambda}_d$. Define the tracking error of reconstructed flux and error of estimated integration constant accordingly as $\widetilde{\boldsymbol{\lambda}} = \widehat{\boldsymbol{\lambda}} - \boldsymbol{\lambda}_d$ and $\widetilde{\mathbf{A}} = \mathbf{A} - \widehat{\mathbf{A}}$. From (9), we obtain

$$\begin{aligned}\dot{\widetilde{\boldsymbol{\lambda}}} &= \dot{\boldsymbol{\lambda}} + \dot{\widehat{\mathbf{A}}} - \dot{\boldsymbol{\lambda}}_d \\ &= (\tfrac{\pi}{\tau} v\mathbf{J}_2 - \tfrac{R_r}{L_r}\mathbf{I}_2 - \tfrac{L_m R_r}{L_r} k_\lambda)\widetilde{\boldsymbol{\lambda}} + \left(\tfrac{\pi}{\tau} v\mathbf{J}_2 \right. \\ &\quad \left. - \tfrac{R_r}{L_r}\mathbf{I}_2\right)\widetilde{\mathbf{A}} + \tfrac{L_m}{L_r} R_r \alpha_2 \widetilde{\mathbf{i}} + \boldsymbol{\xi}_\lambda - \boldsymbol{\varsigma} \end{aligned} \quad (20)$$

where $\widetilde{\mathbf{i}} \equiv \mathbf{i} - \mathbf{i}^*$; $k_\lambda > 0$; $\boldsymbol{\varsigma}$ is an auxiliary signal determined later; and $\boldsymbol{\xi}_\lambda = (\tfrac{\pi}{\tau} v\mathbf{J}_2 - \tfrac{R_r}{L_r}\mathbf{I}_2)\boldsymbol{\lambda}_d + \tfrac{L_m R_r}{L_r} k_\lambda \widetilde{\boldsymbol{\lambda}} + \tfrac{L_m}{L_r} R_r \alpha_2 \mathbf{i}^* + \dot{\widehat{\mathbf{A}}} - \dot{\boldsymbol{\lambda}}_d + \boldsymbol{\varsigma}$. Since $\boldsymbol{\xi}_\lambda$ is a perturbation term in (20), set $\boldsymbol{\xi}_\lambda = 0$ to determine $\mathbf{i}^*$ and ρ. From definition of $\boldsymbol{\lambda}_d$, we obtain

$$\begin{aligned}\mathbf{i}^* &= \tfrac{1}{\alpha_2}\left(\tfrac{L_r}{L_m R_r}((\dot{\rho} - \tfrac{\pi}{\tau} v)\mathbf{J}_2\boldsymbol{\lambda}_d - \dot{\widehat{\mathbf{A}}} - \boldsymbol{\varsigma}) \right. \\ &\quad \left. + \tfrac{1}{L_m}\boldsymbol{\lambda}_d - k_\lambda \widetilde{\boldsymbol{\lambda}}\right), \end{aligned} \quad (21)$$

where the relation $\dot{\boldsymbol{\lambda}}_d = \dot{\rho}(t)\,\mathbf{J}_2\boldsymbol{\lambda}_d$ (c.f., C.1) has been used.

Step 2 Substitute (21) into (17) (i.e., satisfying C.2). The result of the substitution along with C.1 is used to determine the angle $\rho(t)$ where

$$\begin{aligned}\dot{\rho}(t) &= \tfrac{\pi}{\tau} v + \tfrac{1}{c^2}\left(R_r(\tfrac{\tau F_d}{\pi n_p} + \tfrac{L_m}{L_r} k_\lambda \widetilde{\boldsymbol{\lambda}}^{\mathrm{T}}\mathbf{J}_2\boldsymbol{\lambda}_d) \right. \\ &\quad \left. + (\dot{\widehat{\mathbf{A}}} + \boldsymbol{\varsigma})^{\mathrm{T}}\mathbf{J}_2\boldsymbol{\lambda}_d\right). \end{aligned} \quad (22)$$

Therefore $\mathbf{i}^*$ can be rewritten in terms of F_d:

$$\mathbf{i}^* = \tfrac{1}{\alpha_2}(\tfrac{1}{L_m}(\mathbf{I}_2 + \tfrac{1}{c^2}\psi\mathbf{J}_2)\boldsymbol{\lambda}_d - \tfrac{L_r}{L_m R_r}(\dot{\widehat{\mathbf{A}}} + \boldsymbol{\varsigma}) - k_\lambda\widetilde{\boldsymbol{\lambda}}) \quad (23)$$

, where $\psi = (L_m k_\lambda \widetilde{\boldsymbol{\lambda}})^{\mathrm{T}}\mathbf{J}_2\boldsymbol{\lambda}_d + L_r(\tfrac{\tau F_d}{\pi n_p} + \tfrac{1}{R_r}(\dot{\widehat{\mathbf{A}}} + \boldsymbol{\varsigma})^{\mathrm{T}}\mathbf{J}_2\boldsymbol{\lambda}_d)$.

5. Adaptive mechanism and stability analysis

Based on the control law (23), the error dynamics (16) and (20) are further expressed as

$$\begin{aligned} & M\dot{\tilde{v}} + (D + k_v)\,\tilde{v} \\ &= \tfrac{\pi L_m n_p}{\tau L_r}\left(\alpha_2 \mathbf{i}^{\mathrm{T}}\mathbf{J}_2\widetilde{\boldsymbol{\lambda}} + \alpha_2 \mathbf{i}^{\mathrm{T}}\mathbf{J}_2\widetilde{\mathbf{A}} \right. \\ &\quad \left. + \alpha_2 \widetilde{\mathbf{i}}^{\mathrm{T}}\mathbf{J}_2\boldsymbol{\lambda}_d\right) - \mathbf{Y}\widetilde{\boldsymbol{\theta}} \end{aligned} \quad (24)$$

$$\begin{aligned}\dot{\widetilde{\boldsymbol{\lambda}}} &= (\tfrac{\pi}{\tau} v\mathbf{J}_2 - \tfrac{R_r}{L_r}\mathbf{I}_2 - \tfrac{L_m R_r}{L_r} k_\lambda)\widetilde{\boldsymbol{\lambda}} + \\ &\quad + \left(\tfrac{\pi}{\tau} v\mathbf{J}_2 - \tfrac{R_r}{L_r}\mathbf{I}_2\right)\widetilde{\mathbf{A}} + \tfrac{L_m}{L_r} R_r \alpha_2 \widetilde{\mathbf{i}} - \boldsymbol{\varsigma} \end{aligned} \quad (25)$$

where (11) and (17) have also been used. The semi-current-fed LIM is carried out by taking the current error $(\mathbf{i} - \mathbf{i}^*)$ as the input of the PI current controller (12) and (13). We now show that the tracking errors $\tilde{v}$ and $\widetilde{\boldsymbol{\lambda}}$ are convergent once update laws for $\widehat{\boldsymbol{\theta}}$ and $\widehat{\mathbf{A}}$ are suitably chosen. Consider a Lyapunov function candidate as

$$V = \tfrac{1}{2}\alpha M\tilde{v}^2 + \tfrac{1}{2}\alpha\widetilde{\boldsymbol{\theta}}^{\mathrm{T}}\boldsymbol{\Gamma}_2^{-1}\widetilde{\boldsymbol{\theta}} + \tfrac{1}{2}(\widetilde{\boldsymbol{\lambda}}^{\mathrm{T}}\widetilde{\boldsymbol{\lambda}} + \widetilde{\mathbf{A}}^{\mathrm{T}}\boldsymbol{\Gamma}_1^{-1}\widetilde{\mathbf{A}}) \quad (26)$$

where α is an arbitrary positive constant; and $\boldsymbol{\Gamma}_1 = \boldsymbol{\Gamma}_1^{\mathrm{T}}$, $\boldsymbol{\Gamma}_2 = \boldsymbol{\Gamma}_2^{\mathrm{T}}$ are positive definite adaptation gains. The time derivative of (26) is

$$\begin{aligned}\dot{V} &= -\alpha(D + k_v)\tilde{v}^2 - \tfrac{R_r}{L_r}(1 + L_m k_\lambda)\widetilde{\boldsymbol{\lambda}}^{\mathrm{T}}\widetilde{\boldsymbol{\lambda}} + \alpha\widetilde{\boldsymbol{\theta}}^{\mathrm{T}} \\ &\quad \left(\boldsymbol{\Gamma}_2^{-1}\dot{\widetilde{\boldsymbol{\theta}}} - \tilde{v}\mathbf{Y}^{\mathrm{T}}\right) + \widetilde{\mathbf{A}}^{\mathrm{T}}\left(\boldsymbol{\Gamma}_1^{-1}\dot{\widetilde{\mathbf{A}}} + \tfrac{\pi}{\tau} v\mathbf{J}_2^{\mathrm{T}}\widetilde{\boldsymbol{\lambda}} - \tfrac{R_r}{L_r}\widetilde{\boldsymbol{\lambda}} \right. \\ &\quad \left. + \tfrac{\alpha\pi L_m n_p}{\tau L_r}\tilde{v}\mathbf{J}_2^{\mathrm{T}}\alpha_2\mathbf{i}\right) + \widetilde{\boldsymbol{\lambda}}^{\mathrm{T}}\left(\tfrac{\alpha\pi L_m n_p}{\tau L_r}\tilde{v}\mathbf{J}_2^{\mathrm{T}}\alpha_2\mathbf{i} - \boldsymbol{\varsigma}\right) \\ &\quad + \tfrac{L_m}{L_r}\alpha_2\widetilde{\mathbf{i}}^{\mathrm{T}}(\alpha\tfrac{\pi}{\tau} n_p\tilde{v}\mathbf{J}_2\boldsymbol{\lambda}_d + R_r\widetilde{\boldsymbol{\lambda}}). \end{aligned}$$

The update laws for $\widehat{\mathbf{A}}$ and $\widehat{\boldsymbol{\theta}}$ are

$$\dot{\widehat{\mathbf{A}}} = \boldsymbol{\Gamma}_1(\tfrac{\pi}{\tau} v\mathbf{J}_2^{\mathrm{T}}\widetilde{\boldsymbol{\lambda}} - \tfrac{R_r}{L_r}\widetilde{\boldsymbol{\lambda}} + \tfrac{\alpha\pi L_m n_p}{\tau L_r}\tilde{v}\mathbf{J}_2^{\mathrm{T}}\alpha_2\mathbf{i}) \quad (27)$$

$$\dot{\widehat{\boldsymbol{\theta}}} = -\tilde{v}\boldsymbol{\Gamma}_2\mathbf{Y}^{\mathrm{T}} \quad (28)$$

The auxiliary signal $\boldsymbol{\varsigma}$ is given as

$$\boldsymbol{\varsigma} = \tfrac{\alpha\pi L_m n_p}{\tau L_r}\tilde{v}\mathbf{J}_2^{\mathrm{T}}\alpha_2\mathbf{i} \quad (29)$$

As a result, we arrive with the following equation

$$\begin{aligned}\dot{V} &\le -\alpha(D + k_v)\tilde{v}^2 - \tfrac{R_r}{L_r}(1 + L_m k_\lambda)\widetilde{\boldsymbol{\lambda}}^{\mathrm{T}}\widetilde{\boldsymbol{\lambda}} \\ &\quad + \tfrac{L_m}{L_r}\alpha_2\widetilde{\mathbf{i}}^{\mathrm{T}}\begin{bmatrix} \alpha\tfrac{\pi}{\tau} n_p\mathbf{J}_2\boldsymbol{\lambda}_d & R_r\mathbf{I}_2 \end{bmatrix}\begin{bmatrix} \tilde{v} \\ \widetilde{\boldsymbol{\lambda}} \end{bmatrix} \end{aligned} \quad (30)$$

Theorem: *Consider a semi-current-fed LIM use virtual desired flux with $\rho(t)$ as (22), and control law (23). The estimated parameters are updated by (27)∼(28). If the control gains k_v, k_λ, c and α are suitably chosen, the closed-loop control system has the following properties:*

(a) If A.1∼A.6 are satisfied, all signals in the model are bounded. Moreover, the tracking errors $\tilde{v}$ and $\widetilde{\boldsymbol{\lambda}}$ with respect to the current error $\widetilde{\mathbf{i}}$ is finite-gain L_2 stable, i.e., $\int_0^t \|\mathbf{z}(\tau)\|^2 d\tau \le \epsilon_1 + \epsilon_2\int_0^t \left\|\widetilde{\mathbf{i}}(\tau)\right\|^2 d\tau$ for $\mathbf{z} = [\tilde{v}\ \widetilde{\boldsymbol{\lambda}}^{\mathrm{T}}]^{\mathrm{T}}$ and some positive constants ϵ_1 and ϵ_2.

(b) If A.1', A.2∼A.6 are satisfied, then the tracking errors $\tilde{v}$ and $\widetilde{\boldsymbol{\lambda}}$ asymptotically converge to zero as $t \to \infty$.

Proof. Part (a): From (30), we have

$$\dot{V} \le -\varepsilon\|\mathbf{z}\|^2 + k\left\|\widetilde{\mathbf{i}}\right\|\|\mathbf{z}\| \quad (31)$$

where $\varepsilon = \min\left(\alpha(D + k_v), \tfrac{R_r}{L_r}(1 + L_m k_\lambda)\right)$, and $k = \tfrac{L_m}{L_r}\sup_t \|[\alpha_2\alpha n_p\mathbf{J}_2\boldsymbol{\lambda}_d\ \alpha_2 R_r\mathbf{I}_2]\| < \infty$. Here the norm of matrix $\tfrac{L_m}{L_r}[\ \alpha_2\alpha n_p\mathbf{J}_2\boldsymbol{\lambda}_d \quad \alpha_2 R_r\mathbf{I}_2\ ]$ depends on c which is

the magnitude of virtual desired flux and electrical parameters L_r, L_m, R_r. Therefore k is upper bounded by a constant. In this case, (31) is rewritten as

$$\begin{aligned}\dot{V} &\leq -(1-\delta)\varepsilon\|\mathbf{z}\|^2 - \delta\varepsilon\|\mathbf{z}\|^2 + k\left\|\widetilde{\mathbf{i}}\right\|\|\mathbf{z}\| \\ &\leq -(1-\delta)\varepsilon\|\mathbf{z}\|^2 \end{aligned} \quad (32)$$

where $0<\delta<1$, $\forall\ \|\mathbf{z}\| \geq \left(k\left\|\widetilde{\mathbf{i}}\right\|/\delta\varepsilon\right)$. This means if $\widetilde{\mathbf{i}} \in L_\infty$ and $\|\mathbf{z}\| \geq \left(k\left\|\widetilde{\mathbf{i}}\right\|/\delta\varepsilon\right)$, then $\dot{V}\leq 0$. Hence we conclude V is upper bounded, whereas error signals $\tilde{v}$ and $\widetilde{\boldsymbol{\lambda}}$ are uniformly bounded. In other words, $\tilde{v}$, $\widetilde{\boldsymbol{\lambda}} \in L_\infty$ and all parametric errors $\widetilde{\mathbf{A}}$ and $\widetilde{\boldsymbol{\theta}} \in L_\infty$. Due to $\boldsymbol{\lambda} = \widehat{\boldsymbol{\lambda}} + \widetilde{\mathbf{A}}$ and $\widehat{\boldsymbol{\lambda}}$, $\widetilde{\mathbf{A}} \in L_\infty$, the secondary flux $\boldsymbol{\lambda}$ is therefore uniformly bounded. The investigation remains on the boundedness of signals $\mathbf{i}^*$ and $\dot{\rho}(t)$. Consider the dynamics of the current in (8) rewritten as

$$\begin{aligned}&\beta p(\alpha_2\mathbf{i}) + \left(\tfrac{R_rL_m}{L_r}\alpha_2 + \tfrac{R_sL_r}{L_m} + \tfrac{L_r}{L_m}\alpha_1\right)\mathbf{i} \\ =\ & -\left(\tfrac{\pi}{\tau}v\mathbf{J}_2 - \tfrac{R_r}{L_r}\mathbf{I}_2\right)\boldsymbol{\lambda} + \tfrac{L_r}{L_m}\mathbf{V}_s \end{aligned} \quad (33)$$

From A.1, the current-loop induces the primary voltage $\mathbf{V}_s$ to be uniformly bounded. Therefore v, $\boldsymbol{\lambda}$, $\mathbf{V}_s \in L_\infty$ leads to the left-hand side of (33) to be uniformly bounded. Furthermore, (33) is taken as a stable filter driven by a bounded input. Thus the state $\mathbf{i}$ is uniformly bounded. In addition to the fact that $\tilde{v}$, $\widetilde{\boldsymbol{\lambda}}$, $\mathbf{i} \in L_\infty$, signals $\mathbf{i}^*$ and $\dot{\rho}(t)$; update laws $\dot{\widehat{\boldsymbol{\theta}}}$, $\dot{\widehat{\mathbf{A}}}$; and auxiliary $\boldsymbol{\varsigma}$ are uniformly bounded. Finally from the above analysis, we conclude that all signals on the right–hand sides of (24) and (25) are bounded, which means $\mathbf{z}$ and $\dot{\mathbf{z}}$ are uniformly bounded.

Furthermore considering (30) and facts

$$\begin{aligned}\tfrac{\alpha\pi L_m n_p}{\tau L_r}\tilde{v}\alpha_2\widetilde{\mathbf{i}}^{\mathrm{T}}\mathbf{J}_2\boldsymbol{\lambda}_d &\leq \tfrac{\alpha^2\pi^2c^2n_p^2}{\tau^2R_r}\tilde{v}^2 + \tfrac{\alpha_2^2L_m^2R_r}{4L_r^2}\widetilde{\mathbf{i}}^{\mathrm{T}}\widetilde{\mathbf{i}} \\ \tfrac{L_mR_r}{L_r}\alpha_2\widetilde{\mathbf{i}}^{\mathrm{T}}\widetilde{\boldsymbol{\lambda}} &\leq R_r\widetilde{\boldsymbol{\lambda}}^{\mathrm{T}}\widetilde{\boldsymbol{\lambda}} + \tfrac{\alpha_2^2L_m^2R_r}{4L_r^2}\widetilde{\mathbf{i}}^{\mathrm{T}}\widetilde{\mathbf{i}},\end{aligned}$$

we are able to rewrite $\dot{V}$ as

$$\begin{aligned}\dot{V} &\leq -\alpha\left(D + k_v - \tfrac{\alpha\pi^2c^2n_p^2}{\tau^2R_r}\right)\tilde{v}^2 \\ &\quad -\tfrac{R_r}{L_r}(1 + L_mk_\lambda - L_r)\widetilde{\boldsymbol{\lambda}}^{\mathrm{T}}\widetilde{\boldsymbol{\lambda}} + \tfrac{\alpha_2^2L_m^2R_r}{2L_r^2}\left\|\widetilde{\mathbf{i}}\right\|^2 \\ &= -\mathbf{z}^{\mathrm{T}}\mathbf{Q}\mathbf{z} + \tfrac{\alpha_2^2L_m^2R_r}{2L_r^2}\left\|\widetilde{\mathbf{i}}\right\|^2 \end{aligned} \quad (34)$$

where

$$\begin{aligned}\mathbf{Q} &= diag\left\{\alpha(D + k_v - \tfrac{\alpha\pi^2c^2n_p^2}{\tau^2R_r}) \right. \\ &\quad \left., \tfrac{R_r}{L_r}(1 + L_mk_\lambda - L_r)\mathbf{I}_2\right\}\end{aligned}$$

Note that $\mathbf{Q}$ is positive definite in accordance to properly chosen k_v, k_λ, c and α. Integrating on both sides of (34) leads to

$$\begin{aligned}\int_0^t \mathbf{z}^{\mathrm{T}}\mathbf{Q}\mathbf{z}d\tau &\leq V(0) - V(t) + \tfrac{\alpha_2^2L_m^2R_r}{2L_r^2}\int_0^t\left\|\widetilde{\mathbf{i}}\right\|^2 d\tau \\ &\leq V(0) + \tfrac{\alpha_2^2L_m^2R_r}{2L_r^2}\int_0^t\left\|\widetilde{\mathbf{i}}\right\|^2 d\tau \end{aligned} \quad (35)$$

and thus completes the proof of (a).

Part (b): From A.1', it follows that $\widetilde{\mathbf{i}} \in L_2$. Now, form the result of Part (a), we have $\mathbf{z} \in L_2$ by (35). According to $\mathbf{z}$, $\dot{\mathbf{z}} \in L_\infty$, $\mathbf{z} \in L_2$ and applying Barbalat's lemma, it is concluded that $\lim_{t\to\infty}\mathbf{z}(t)$. In other words, $\tilde{v}$ and $\widetilde{\boldsymbol{\lambda}}$ asymptotically converges to zero as $t\to\infty$ without the persistent excitation condition nor using an observer. ■

Since the secondary flux tracking error $(\boldsymbol{\lambda} - \boldsymbol{\lambda}_d)$ equals to $\left(\widetilde{\boldsymbol{\lambda}} + \widetilde{\mathbf{A}}\right)$, $\widetilde{\mathbf{A}} \to 0$ is required to achieve $\boldsymbol{\lambda} \to \boldsymbol{\lambda}_d$ as $t\to\infty$. In traditional adaptive approaches, zero parameter errors are obtained only if the PE condition is satisfied. Here we can further show that $\boldsymbol{\lambda}$ tracks $\boldsymbol{\lambda}_d$ when PE condition succeeds.

6. Experimental results

The LIM parameters expressed in per unit values: rated output power = 1 HP; pole pair = 2; rated voltage V_s = 240 V; rated current I_s = 5 A; primary length D_l = 0.24 m; pitch τ = 0.465 m; nominal value of M = 4.775 Kg; D = 53 Kg/sec; R_s = 13.2 Ω; R_r = 11.78 Ω; L_s = 0.42 H; L_r = 0.42 H; L_m = 0.4 H. The control parameters are chosen as: $k_p = -450$, $k_i = -350$, $\alpha = 0.045$, $k_v = 300.5$, $k_\lambda = 2.1$ and $c = 25.61$. Update gains are set as $\boldsymbol{\Gamma}_1 = 0.8$, $\boldsymbol{\Gamma}_2 = diag\left\{3e^1, 3e^{-5}, 3e^{-4}, 3e^{-2}, 0.86\right\}$. We first consider speed regulation for $v_d = 15(1 - e^{-10t})$ cm/sec. The speed reference, speed response, and speed error are shown in Fig. 2(a), 2(b), 2(c), respectively; the primary voltage and primary current are shown in Fig. 2(d), 2(e). Secondly, the reference speed is set at $v_d = 15\sin(2\pi t)$ cm/sec. The speed reference, speed response, and speed error are shown in Fig. 3(a), 3(b), 3(c), respectively, the primary voltage and primary current are shown in Fig. 3(d), 3(e).

7. Conclusions

In this paper, a complete mathematical model of an LIM is derived. A *semi-current-fed* model for LIM is then introduced. Based on the more practical model, an adaptive controller for speed tracking is derived by using a VDV synthesis method. The experimental results exhibit satisfactory performance. Results with small overshoot, fast transient behavior, and negligible steady-state error are obtained.

Acknowledgments

This work was supported by the National Science Council, R.O.C., under Grant NSC-90-2213-E-033-018.

References

[1] C. I. Huang, K. L. Chen, H. T. Lee, and L.C. Fu, "Nonlinear adaptive motion control of linear induction motor," *Proc. of the American Control Conf.*, pp. 3099-3104, 2002.

[2] H. K. Khalil, *Nonlinear Systems 2nd ed.* New York: Macmillan, 1996.

[3] K. Y. Lian, C. Y. Hung, J. J. Liou, and P. Liu, "Adaptive speed control with friction compensation for semi-current-fed induction motors," *Proceedings of the 15th IFAC World Congr.*, Barcelona, Spain, 2002.

[4] R. Marino, S. Peresada, and P. Tomei, "Output feedback control of current-fed induction motor with unknown rotor resistance," *IEEE Trans. Control System Technology*, vol. 4, pp. 336-347, 1996.

[5] J. H. Sung and K. Nam, "A new approach to vector control for a linear induction motor considering end effects," *Proc. IEEE Conf. Industry Application*, vol. 4, pp. 2284-2289, 1999.

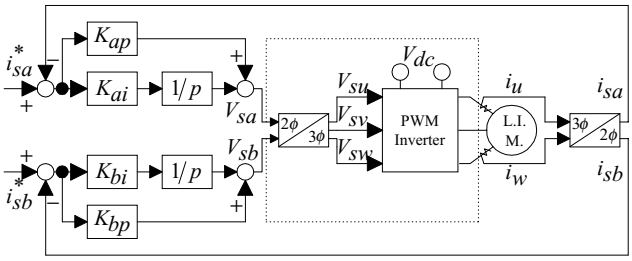

Fig. 1 The control block diagram of an LIM.

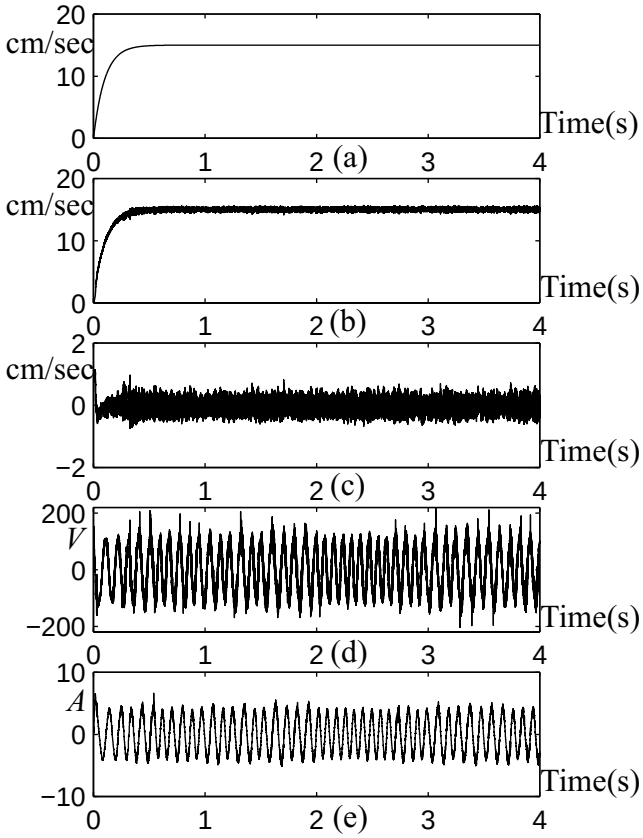

Fig. 2 Experiment results for speed regulation.

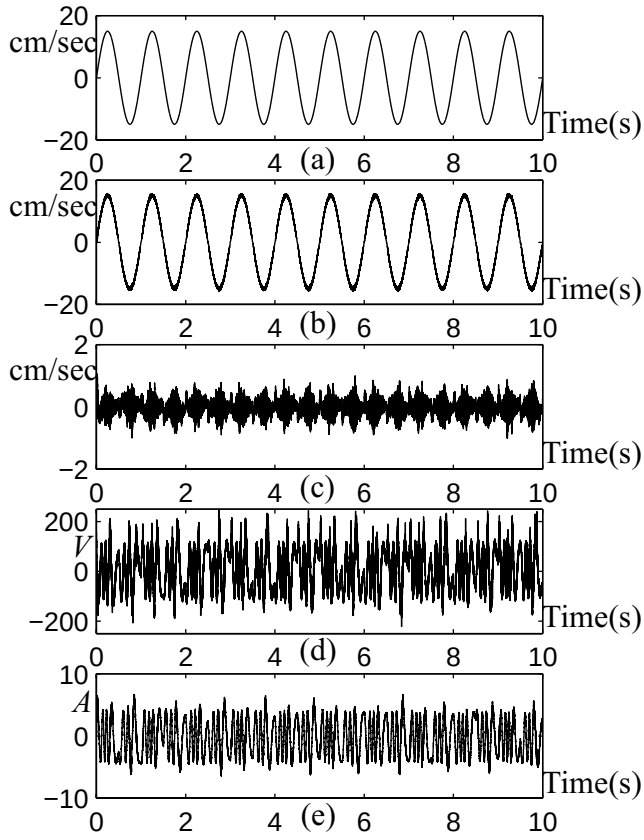

Fig. 3 Experiment results for speed tracking.